Robotica (2010) volume 28, pp. 253–258. © Cambridge University Press 2009
doi:10.1017/S0263574709990671

A hybrid robot system for CT-guided surgery

Da Liu*, Tianmiao Wang, Can Tang and Fan Zhang

Robotics Institute, School of Mechanical Engineering and Automation, Beihang University, Beijing 100191, P.R. China

(Received in Final Form: October 27, 2009. First published online: December 7, 2009)

SUMMARY

The common serial robot or parallel robot is difficult to implement for CT-guided surgery in a limited workspace. A novel hybrid robot with 9 degrees of freedom is presented in this paper, whose detailed structure is analysed based on screw theory and displacement manifold (DM). The dexterity of the hybrid robot is provided in terms of Riemann manifold (RM). Besides, DICOM (digital imaging communications in medicine) image processing, spatial registration and 3D dynamic reconstruction in the operation planning subsystem are analysed, in which some innovative methods are introduced. Meanwhile, the architecture of the CT-guided hybrid robot system and its subsystems are proposed. Simulative clinical experiment showed that the locating precision of the hybrid robot reaches 1.08 mm, which can meet the requirement of CT-guided surgery.

KEYWORDS: Surgical robot; CT-guided surgery; Hybrid robot; Screw theory; Riemann manifold; Operation planning; Clinical experiment.

1. Introduction

Within the last two decades, robot-assisted surgery developed rapidly and has become a promising interdisciplinary field, which has already begun to develop potential applications in surgery.[1] Especially in recent years, with the development of digital imaging technology, CT-guided surgery has been widely applied in many areas, including orthopaedics, endoscopic surgery, neurosurgery and radiosurgery.[2] Compared with traditional operation, this kind of operation has many advantages: real-time operation locating, less injury to healthy tissues, more comfort for patients during and after the operation, shorter recovery time, less expenditure on hospitalization, etc.

But in CT-guided surgery, the locating precision of manually locating surgical tools is very low and unstable. Both the operation space and the motion space of the surgical tools are limited. The X-rays emitted during CT is very harmful to patients and surgeons in a longtime operation.[3] And because of the iterative adjustment of the position and pose of surgical tools, the operation efficiency decreases remarkably. All these disadvantages have hindered the progress of minimally invasive surgery.

* Corresponding author. E-mail: drliuda@yahoo.com.cn

The smart combination of robotics and surgery is one of the main solutions to the above problems. There are two types of robot structure, i.e. serial robots and parallel robots. Serial robots have high dexterity, but low stiffness and precision, while parallel robots have good stiffness and precision, but limited dexterity.

Nowadays, robots have been developed in different countries for performing CT-guided surgery. In 1987, with the help of the industrial robot PUMA200, scientists in the University of Southern California, USA, conducted a biopsy of an intracranial tumor,[4] which was the first CT-guided robot-assisted surgery. In 2002, the 9-DOF (degrees of freedom) serial robot Acrobot[5] was developed in England for knee replacement surgery. A year later, Johns Hopkins Hospital and Georgetown University developed a 9-DOF serial robot system named AcuBot[6] (PAKY-RCM) for percutaneous intervention. Later on in 2004, the 3P-2R-2R serial robot system SPINEBOT[7] was developed for spine surgery.

The dimension of a typical CT is about 700 mm in diameter and 600 mm in depth. The diameter of the head or the abdomen is usually more than 200 mm. So the real operation space is about $400 \times 200 \times 300$ mm^3, which is a narrow workspace for robot movement. In such a limited space, it is difficult for serial robots, such as Acorbot, AcuBot and SPINEBOT,[5–7] to complete an operation because of their large dimension, low stiffness and accumulative error. A traditional parallel robot, such as a Stewart platform, is also difficult to implement because of its low dexterity and manoeuvrability, which cannot meet the demand of puncturing route planning in CT-guided surgery.

In other words, neither serial robots nor parallel robots can satisfy the requirements of CT-guided surgery in a limited space. Therefore, a hybrid robot with a novel structure that has the advantages of both serial and parallel structures must be developed. The ideal design of a hybrid robot would be that along with the precondition of meeting the requirement of operation task space, the robot should also be compact, portable, stiff and dexterous enough to satisfy the requirement of task dexterity (TD).[8] The serial machine of a hybrid robot implements position locating in a large area and also improves the dexterity of the hybrid robot. The parallel machine accomplishes pose locating in a narrow operation area and also improves the robot's stiffness and stability.

In this paper, a new 9-DOF hybrid robot for CT-guided surgery is presented and designed. The hybrid robot consists of a robot locating subsystem and an operation planning

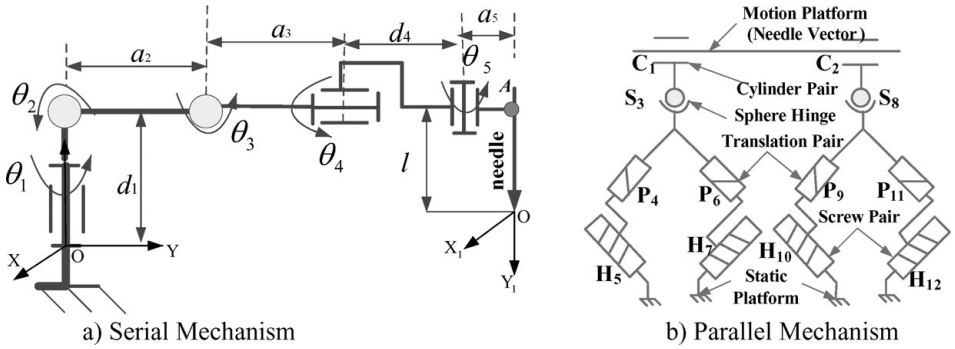

Fig. 1. Topological structure of the hybrid robot.

subsystem. Some novel implementation methods are proposed. The locating precision of the hybrid robot is proved by a simulative clinical experiment. The characteristics of a hybrid-robot-assisted surgery system are also summarized.

2. Robot Locating Subsystem

2.1. Topological structure analysis for serial robot

The joint-coordinate robot has a small size, a big workspace and a large orientation range. All of these are necessary in percutaneous surgery with a CT-guided robot. Therefore, the joint-coordinate structure is adopted in serial robots.

The dexterities of three kinds of serial robots, 3R, 4R and 5R, were compared. Their TDs were found to be 39.8%, 45.6% and 68.6% respectively via MATLAB simulation. The TD of the 5R mechanism was much higher than that of the 3R and 4R mechanisms. So the 5R mechanism was selected as the serial part of the hybrid robot. Figure 1a shows the 5R topological structure. In terms of screw theory, the characteristic function of the displacement output can be deduced as follows (see ref. [9] for details on symbol description):

$$
\begin{aligned}
M_S = &\begin{bmatrix} t^0 \\ r^1(\mathrm{R}_1) \end{bmatrix}_{\mathrm{R}_1} + \begin{bmatrix} \{t^1(\perp \mathrm{R}_2, \rho_{\mathrm{R}_2})\} \\ r^1(//\mathrm{R}_2) \end{bmatrix}_{\mathrm{R}_2} \\
&+ \begin{bmatrix} \{t^1(\perp \mathrm{R}_3, \rho_{\mathrm{R}_3})\} \\ r^1(//\mathrm{R}_3) \end{bmatrix}_{\mathrm{R}_3} + \begin{bmatrix} t^1(\perp \mathrm{R}_4, \rho_{\mathrm{R}_4}) \\ \{r^1(//\mathrm{R}_4)\} \end{bmatrix}_{\mathrm{R}_4} \\
&+ \begin{bmatrix} t^1(\perp \mathrm{R}_5, \rho_{\mathrm{R}_5}) \\ \{r^1(//\mathrm{R}_5)\} \end{bmatrix}_{\mathrm{R}_5} + \begin{bmatrix} t^1(\perp \mathrm{R}_6, \rho_{\mathrm{R}_6}) \\ \{r^1(//\mathrm{R}_6)\} \end{bmatrix}_{\mathrm{R}_6} \\
= &\begin{bmatrix} t^3 \\ r^3 \end{bmatrix}_6 . \qquad (2.1)
\end{aligned}
$$

2.2. Topological structure analysis for parallel robot

Here, a new structure for parallel robots with high dexterity is proposed, as shown in Fig. 1b. The four screw pairs H_5, H_7, H_{10} and H_{12} are directly linked with the static platform. The plane determined by H_5 and H_7 is parallel to the plane determined by H_{10} and H_{12}. From the single chain, H_5 is perpendicular to P_4, and it is joined to P_4 as well. H_7 with P_6 is similar. P_4 and P_6 are normal to each other. The cylinder pair C_1 and spherical hinge S_3 are connected to each other and are coaxial. In fact, the dynamic platform of the parallel mechanism is a needle, which could be simplified as a spatial vector.

There are two single chains linked to each other from the static platform to the dynamic platform, namely C_1-S_3-P_4-H_5 (or C_1-S_3-P_6-H_7) and C_2-S_8-P_9-H_{10} (or C_2-S_8-P_{11}-H_{12}). According to the definition given by Professor Zhen[10] at Yanshan University, Professor Murray[11] and Sorli and Ferraresi[12] it is certain that the mechanism belongs to the parallel robot. The characteristic function of displacement output can be deduced as follows:

$$
\begin{aligned}
M_{\mathrm{pa}} = &\begin{bmatrix} t^1(//\mathrm{H}_5) \\ r^0 \end{bmatrix}_{11} + \begin{bmatrix} t^1(//\mathrm{H}_7) \\ r^0 \end{bmatrix}_{12} + \begin{bmatrix} t^0 \\ r^1(//\mathrm{R}_3^1) \end{bmatrix}_{13} \\
&+ \begin{bmatrix} t^0 \\ r^1(//\mathrm{R}_3^2) \end{bmatrix}_{14} + \begin{bmatrix} t^0 \\ r^1(//\mathrm{R}_3^3) \end{bmatrix}_{15} + \begin{bmatrix} t^1(//\mathrm{P}_1) \\ r^0(//\mathrm{R}_3^3) \end{bmatrix}_{16} \\
= &\begin{bmatrix} t^3 \\ r^3 \end{bmatrix}_6 . \qquad (2.2)
\end{aligned}
$$

The TD of the parallel robot is about 68.9% via MATLAB calculation.

According to the specific requirements of a CT-guided surgical robot, some design principles can be determined. First, the robot must be small and compact. Second, its structure should not be complex. Third, the robot should be highly dexterous. In CT-guided surgery, all spatial motions except translation along the puncturing needle axis could be implemented by the parallel robot. That is to say, the needle can move with two translations and three rotations (2T-3R). Therefore, the dimension of the displacement subgroup (DS) is five; the dimension of the sub-subgroup is five or six. The displacement manifolds (DMs) of the parallel robot is $\{M\} = \{S(N)\} \cdot \{T(P_{xy})\}$. The equivalent DM of parallel robot is:$\{M\} = \{G(u)\} \cdot \{S(N)\}$. All these DMs can produce 2T-3R motion. The motion synthesis method (MSM) based on DS is then put forward to analyse type synthesis of a lower-mobility parallel mechanism[13] for minimally invasive surgery. Eleven basic DMs of parallel mechanism with a 2T-3R structure are deduced, and 24 sub-manifolds are also set up. Therefore, the fact that there is a DS in this kind of 2T-3R parallel mechanism is validated. The DM of the hybrid robot (see ref. [13] for details on symbol description) is given

https://doi.org/10.1017/S0263574709990671 Published online by Cambridge University Press

Fig. 2. Prototype of the serial robot.

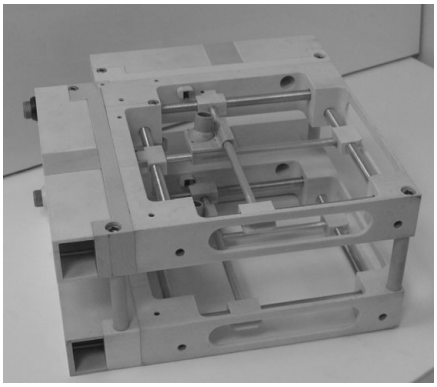

Fig. 3. Prototype of the parallel robot.

in Eq. (2.3).

$$\begin{cases} \{M_{\text{serial}}\} = \{R(N_1, \boldsymbol{u})\} \cdot \{R(N_1, \boldsymbol{v})\} \cdot \{R(N_2, \boldsymbol{v})\} \\ \qquad\qquad \cdot\{R(N_2, \boldsymbol{w}_1)\} \cdot \{R(N_3, \boldsymbol{w}_2)\} \\ \{M_{\text{para}}\} = \{H(N_4, \boldsymbol{u}, p)\} \cdot \{H(N_5, \boldsymbol{u}, p)\} \cdot \{H(N_6, \boldsymbol{u}, p)\} \cdot \\ \qquad\qquad \cdot\{H(N_7, \boldsymbol{u}, p)\} \\ \{M_{\text{hybrid}}\} = \{M_{\text{serial}}\} \cup \{M_{\text{serial}}\} \end{cases} \tag{2.3}$$

2.3. Prototype designs of the serial robot and the parallel robot

The serial robot is designed as a 5-DOF passive arm made from duralumin alloy, featuring the hydraulically locked-up structure with high stiffness. Figure 2 shows the prototype of the serial robot. When the pedal of the serial robot is free, all the five revolving joints are locked up hydraulically in order to support the load brought about by any end manipulators. And if the pedal is being stepped on, hydraulic locking forces will disappear so that the serial robot could be adjusted to desired poses.

Figure 3 shows the prototype of the parallel robot. It consists of a two-layer static platform, a gearbox driven by DC micro-motors, cross screw rails and sphere joints. Each sphere joint can be driven to move on a plane surface respectively in two vertical directions; two of them determine a line vector, namely the puncturing needle path.

2.4. Dexterity analysis for hybrid robot

Figure 4 shows the prototype of the hybrid robot.

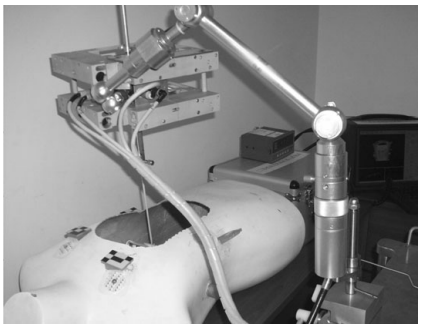

Fig. 4. Prototype of the hybrid robot.

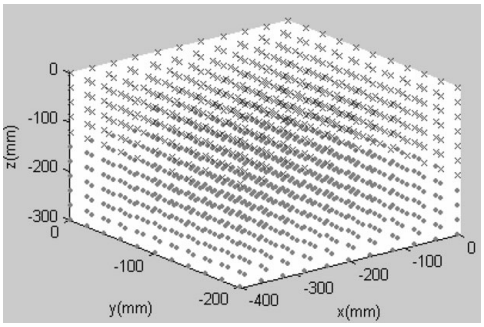

Fig. 5. Dexterity distribution of the hybrid robot.

The traditional method for robot dexterity analysis is based on the analytical solution of inverse kinematics, which is difficult to obtain in a 9-DOF redundant robot. Therefore, a novel dexterity analysis method is presented. With Riemann manifold and Riemann measuring,[14] we can define hybrid robot dexterity: in the workspace, it is the area ratio of Riemann surface formed by the manipulator tip point and by the manipulator end point. The area of Riemann surface could be calculated only by a function of the forward kinematics of the hybrid robot. In surgery workspace, the TD of the hybrid robot is 83.3% (see Fig. 5), which is higher than the required clinical dexterity of 60% for CT-guided surgery. Here, the '+' denotes a dexterous point, and the '×' denotes a non-dexterous point.

Compared with other hybrid medical robots, the proposed hybrid robot has some similar characteristics. First, the 5-DOF passive serial robot is very compact and light, weighing only 7.5 kg, which is an advantage in terms of manipulation and portability. Second, the passive serial robot has a 5R structure, which proves to be very dexterous for pose locating. Third, the passive robot can be locked up hydraulically, the end manipulator of which can stay at any position in the workspace. Fourth, the active robot is designed based on the ideals of modularization and light weight. Besides high rigidity, the active parallel robot has high dexterity, which is helpful for operation planning.

3. Operation Planning Subsystem

The operation planning subsystem consists of spatial registration, DICOM image processing and 3D reconstruction.

The registration between the patient's images and the patient is to establish their spatial relationship to apply

https://doi.org/10.1017/S0263574709990671 Published online by Cambridge University Press

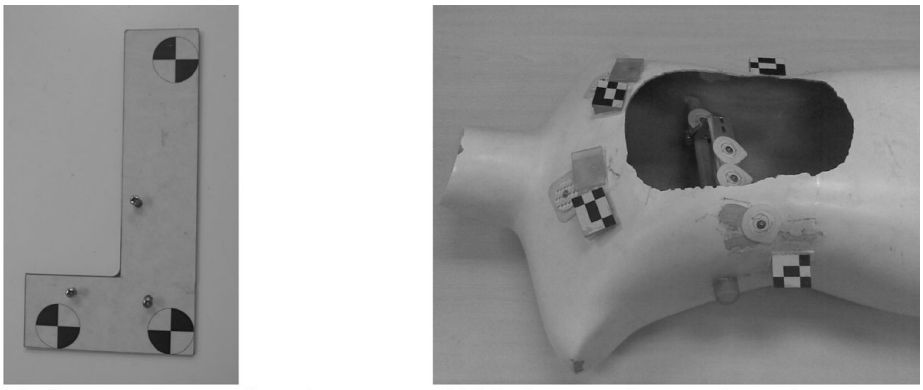

a) Marker template on the robot b) Marker template on the patient

Fig. 6. Marker templates for registration.

the operation planning to the actual patient. First, fiducial markers, which are clearly distinguishable on the images, are attached to the pertinent anatomical structure of the patient prior to imaging. Registration is done by finding the spatial transformation matrix between the image coordinates and the localizer coordinates of the markers, in which the latter is measured during surgery by the optical camera.

The traditional approach is moving the needle tip of the manipulator to 12 pre-designed spatial positions. And by inverse kinematics, the transformation matrix is built up in about 10 min. In our system, transformation matrix could be obtained in no more than a second by using the MicronTracker tracking system. MicronTracker can not only track still objects, but also dynamic targets within its visual region. A marker template was fixed to the object that will be tracked by the MicronTracker, as shown in Figs. 6a and b. The marker templates are designed to be identified by both CT and the MicronTracker. As a result, the MicronTracker can immediately locate the markers by the tracked templates. The method takes less time than the general registration method as there is no need of robot movement and because of the high registration precision of the MicronTracker, which is about 0.25 mm, much higher than that in the traditional method (on average 1.0 mm). Reference [19] introduces the registration algorithm in detail.

CT images of the patient are imported into the planning software and displayed as 2D images. Due to the fluctuation of the marker with the patient's breathing, the marker position is changed along with the movement of the chest. Therefore, a dynamic reconstruction of the patient's focus is important to build up the exact transformation matrix. The main step of dynamic reconstruction is how to get the transfiguration algorithm of the focus polygon. Focus shapes taken at least two different times are needed. Traditional linear interpolation leads to image degeneration and self-intersection. Thomas W. Sederberg[15,16] and Michal Shapira and Ari Rappoport[17] optimized the algorithm, but the time complexity is O (n^4). Hayley N. Iben[18] put forward an opening-puckering algorithm based on a protruding parcel. But the time taken by this algorithm is very long because energy variation needs to be verified in each step. All the above algorithms have a common feature, which is to try to find a corresponding relationship between the original vertex and the ultimate vertex of the polygon.

Here, a novel algorithm is presented, which is independent of the corresponding relationship of polygon vertexes. The algorithm comprises the following steps: First, the polygon is transformed to multi-section fold lines. Then the length proportions of the polygon vertexes on each fold line are calculated. Finally, the corresponding relationship between the original polygon and the ultimate polygon is set up. Figure 7 shows the focus reconstruction process based on this algorithm.

4. Experiment

To measure the overall application accuracy of the robot system, we tested the system on a patient phantom (see Fig. 8). In the experiment, pre-operatively taken CT images were imported to the planning subsystem for space registration and surgical planning. By space registration, it was possible to convert the surgical parameter planned on image-to-robot commands. First, the serial part of the robot was located manually, and then the parallel part was controlled to move to the planned position for puncture. Besides, intra-operative images were needed for dynamic reconstruction of focus. As can be seen, there was no need for a large invasion in using our system, which means that our robot system can achieve the purpose of minimal invasion.

Figure 9 shows the precision experiment. The locating error of single joint and the absolute locating precision are shown in Figs. 10–12. In Fig. 10, the maximum error of single joint of the serial robot is 0.01°. The average error is about 0.0086°. From Fig. 11, we can see that the maximum error and the average error of single joint of the parallel robot are 0.52 mm and 0.42 mm respectively. The absolute locating error is influenced by factors such as mechanical error of robot, spatial registration error, error of image process, etc. We can see from Table I and Fig. 12 that the absolute locating precision is averagely 1.08 mm (clinical operation requires no more than 5 mm). The registration error is described in ref. [19].

5. Summary and Future Work

There are some benefits to the introduction of the hybrid robot in CT-guided surgery. First, it can lessen the influence of hand trembling when surgeons hold surgical tools to operate

https://doi.org/10.1017/S0263574709990671 Published online by Cambridge University Press

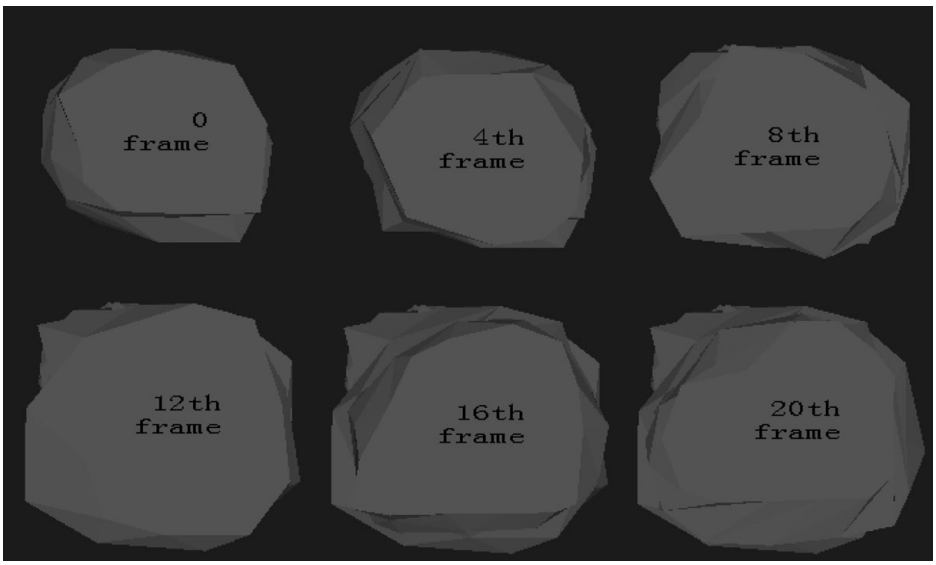

Fig. 7. Dynamic 3D reconstruction course of lung DICOM image.

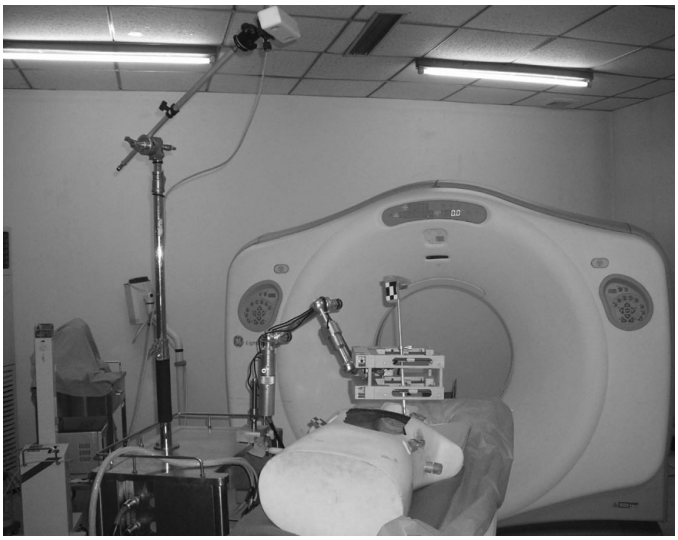

Fig. 8. Simulative clinical experiment.

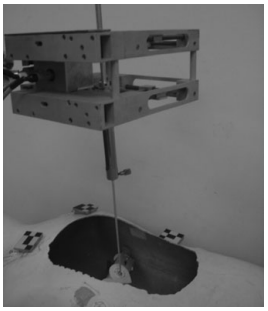

Fig. 9. Precision testing of hybrid robot.

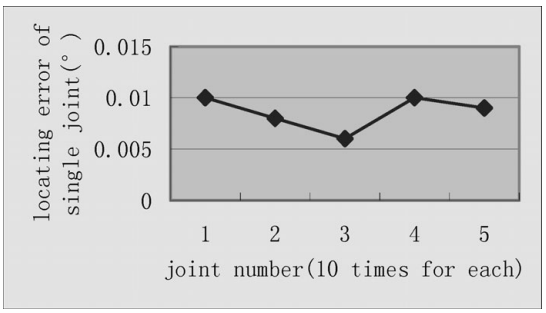

Fig. 10. Locating error of serial robot.

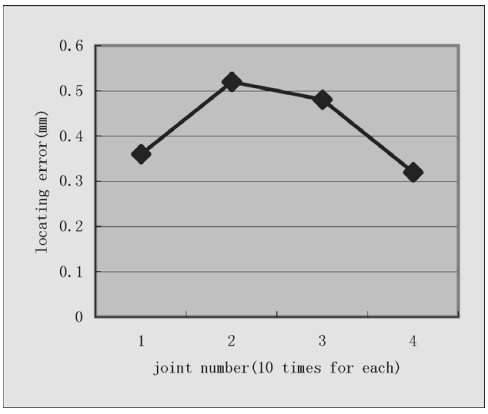

Fig. 11. Locating precision of parallel robot.

and can improve locating precision. Second, compared with traditional spatial registration, time consumption of marker localization is shortened from 10 min to 1 s. Third, the introduction of the hybrid robot can alleviate harm caused by X-ray to operators during CT scanning. Fourth, through the automatic planning of hybrid robot, surgical efficiency is greatly enhanced. Fifth, the hybrid robot system is dexterous for CT-guided surgery in a limited space. A new dexterity analysis method is presented based on Riemann manifold. Last but not the least, some features, such as the hydraulically locked-up structure with high stiffness, markers' automatic capture and compact decoupled (moving orthogonally) parallel mechanism, improve locating precision. Subsequent work that focuses on animal experiment and clinical experiment will follow.

https://doi.org/10.1017/S0263574709990671 Published online by Cambridge University Press

Table I. Precision testing data for hybrid robot.

Testing times (s)	1–10	10–20	20–30	30–40	40–50	50–60	60–70
Precision (mm)	1.22	1.18	0.78	0.96	1.44	1.08	1.26
Testing times (s)	70–80	80–90	90–100	100–110	110–120		Average
Precision (mm)	0.70	0.92	1.12	1.24	1.02		1.08

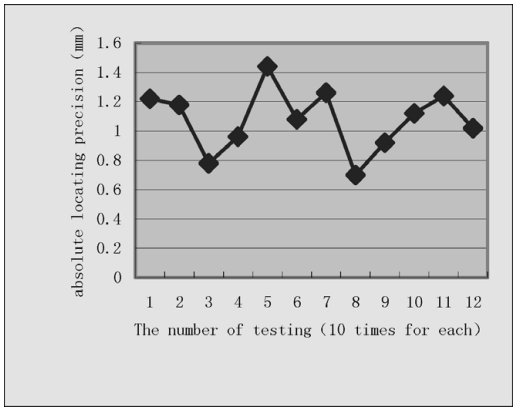

Fig. 12. Locating precision of hybrid robot.

Acknowledgements

This research work was supported by the International Cooperation Project from the Ministry of Science and Technology of People's Republic of China under grant no. 2006DFA1229, the Project of Natural Science Fund under grant no. 60705033, and the National High-tech Program of China under contract no. 2007AA04Z246.

References

1. L.-Y. Zhang and Z. Yong-Shun, "The development existing state and foreground of medical micro-robot," *Machinery [J].* **44**(506), 33–37 (2006).
2. P. Alexandru and S. S. MD, "Robotic kidney and spine percutaneous procedures using a new laser-based CT registration method," *Fourth International Conference on Medical Image Computing and Computer-Assisted Intervention (MICCAI)*, IEEE Press, Utrecht (2001) pp. 14–17.
3. W. Hongwu, D. Yunyou, Z. H. Yanqun, F. Huasong, N. Zhoushan, Y. Xia, L. Haiying, H. Zhihai and T. Shuping, "Percutaneous lung cancer cryotherapy guided by computer tomography," *Journal of Naval Gen. Hosp*. **17**, 8–15 (2004).
4. Y. S. Kwoh, J. Hou, E. A. Jonckheere and S. Hayati, "A robot with improved absolute positioning accuracy for CT guided stereotactic brain surgery," *Trans. Biomed. Eng.* **35**(2), 153–160 (1988).
5. M. Jakopec, S. J. Harris, F. Rodriguez y Baena, P. Gomes and B. L. Davies, "Acrobot: A 'hands-on' robot for total knee replacement surgery," *IEEE, AMC2002*, Maribor, Slovenia (2002) pp. 116–120.
6. D. Stoianovici, K. Cleary, A. Patriciu, D. Mazilu, A. Stanimir, N. Craciunoiu, V. Watson and L. Kavoussi, "AcuBot: A robot for radiological interventions," *IEEE Trans. Robotics Automat.* **19**(5), 927–930 (2003).
7. G. B. Chung, S. G. Lee, S. M. Oh, B.-J. Yi, W. K. Kim, Y. S. Kim, J. I. Park and S. H. Oh, "Development of SPINEBOT for spine surgery," *Proceedings of 2004 IEEE/RSJ International Conference on Intelligent Robots and Systems*, Sendai, Japan (2004) pp. 3942–3947.
8. L. Wei and Z. Yu-ru, "Dexterity analysis and design of robot for neurosurgery," *Mach. Des. Res.* **22**, 39–45 (2006).
9. Y. Tingli, *Topology Structure Design of Robot Mechanisms* (Mechanical Industry Press, Beijing, 2004).
10. H. Zhen, K. Lingfu and F. Yuefa, *Mechanism Theory and Control of Parallel Robot* (Mechanical Industry Press, Beijing, 1997).
11. R. M. Murray, Z. Li and S. S. Sastry, *A Mathematical Introduction to Robotic Manipulation* (CRC Press, Boca Raton, FL, 2000).
12. M. Sorli, C. Ferraresi, M. Kolarski, B. Borovac and M. Vukobratovic, "Mechanics of Turin parallel robot," *Mech. Mach. Theory* **32**, 51–77 (1997).
13. L. Qinchuan, "Type synthesis theory of lower-mobility parallel mechanisms and synthesis of new architectures," *Qin Huangdao* (2003) pp. 103–114.
14. L. Qishao, *Modern Math Foundation* (Beijing: Beihang University Press, 2001) pp. 168–171.
15. T. W. Sederberg and G. Eugene, "A physically based approach to 2D shape blending," *Comput. Graph.* **26**, 25–34 (1992).
16. T. W. Sederberg, G. Peisheng, W. Guojin and M. Hong, "2D shape blending: An intrinsic solution to the vertex path problem," *Comput. Graph.* **27**, 15–18 (1993).
17. M. Shapira and A. Rappoport. "Shape blending using the star-skeleton representation," *IEEE Comput. Graph. Appl.* **15**, 44–51 (1995).
18. H. N. Iben, J. F. O'Brien and D. D. Erik, "Refolding planar polygons," *Proceedings of the 2006 Symposium on Computational Geometry*, Sedona, Arizona (June 2006) pp. 71–79.
19. H. Chen, T. Cao, D. Liu and C. Tang, "An efficient method to realize space registration in image-guided robot-assisted surgery," *ICIRA 2008*, Part I, LNAI 5314, Wuhan, China (Oct. 2008) pp. 744–752.

https://doi.org/10.1017/S0263574709990671 Published online by Cambridge University Press